

# Numerical Calculation of Equivalent Permeability Tensor for Fractured Vuggy Porous Media Based on Homogenization Theory

Zhaoqin Huang\*, Jun Yao, Yajun Li, Chenchen Wang and Xinrui Lv

*School of Petroleum Engineering, China University of Petroleum (Huadong),  
Qingdao 266555, China.*

Received 15 July 2009; Accepted (in revised version) 13 April 2010

Available online 5 August 2010

---

**Abstract.** A numerical procedure for the evaluation of equivalent permeability tensor for fractured vuggy porous media is presented. At first we proposed a new conceptual model, i.e., discrete fracture-vug network model, to model the realistic fluid flow in fractured vuggy porous medium on fine scale. This new model consists of three systems: rock matrix system, fractures system, and vugs system. The fractures and vugs are embedded in porous rock, and the isolated vugs could be connected via discrete fracture network. The flow in porous rock and fractures follows Darcy's law, and the vugs system is free fluid region. Based on two-scale homogenization theory, we obtained an equivalent macroscopic Darcy's law on coarse scale from fine-scale discrete fracture-vug network model. A finite element numerical formulation for homogenization equations is developed. The method is verified through application to a periodic model problem and then is applied to the calculation of equivalent permeability tensor of porous media with complex fracture-vug networks. The applicability and validity of the method for these more general fractured vuggy systems are assessed through a simple test of the coarse-scale model.

**AMS subject classifications:** 35B27, 35Q30, 76S05

**Key words:** Fractured vuggy porous media, equivalent permeability tensor, homogenization, upscaling.

---

## 1 Introduction

Evaluation of the equivalent permeability of fractured vuggy porous media has a great interest in petroleum and geotechnical engineering. Such porous media, which are very

---

\*Corresponding author. *Email addresses:* huangzhqin@gmail.com (Z. Huang), yaojunhdpu@126.com (J. Yao), yajunok@126.com (Y. Li), wcc1220@163.com (C. Wang), xinruiabc@gmail.com (X. Lv)

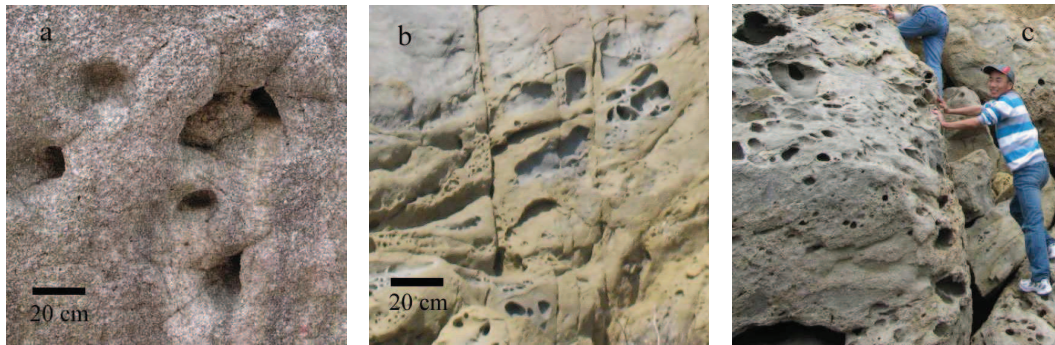


Figure 1: Typical outcrop of fractured vuggy porous media: (a) limestone; (b) dolostone; (c) carbonate rock.

common in the earth's crust especially in carbonate rocks (cf. Fig. 1), contain not only matrix and fractures but also the vugs that are irregular in shape and vary in size from centimeters to meters in diameter [1,2]. The presence of vugs which are connected via discrete fracture networks can significantly increase both the porosity and the permeability of the porous media [3,4]. Although there are reliable methods to estimate porosity and fluid saturation, reliable permeability estimation is difficult for fractured vuggy porous media due to the presence of fractures and vugs at multiple scales. These types of multi-scale rock fabric are difficult to study mainly because they are on a scale that is too large to quantify using thin sections, and frequently on a scale that is too large to quantify adequately using core samples which are only a few centimeters in diameter [5]. Therefore, it is not realistic to predict the effective permeability of these rock fabrics on the field scale using experimental methods.

As an alternative method, numerical upscaling calculation based on accurate geologic models has received much attention recently. While using numerical upscaling calculation methods to evaluate the permeability of porous materials, two important steps should be mentioned. Modeling the fluid flow through fractured vuggy porous media on fine scale is the first step on which the main difficulty is the co-existence of porous flow and free-flow regions. And then, how to incorporate this fine scale data into coarse scale flow properties is the key step. Neal et al. [6] are the pioneers of the related research; they studied the impact of spherical vugs on the permeability in homogeneous isotropic porous media. In their study, creeping Navier-Stokes equation was employed in the spherical cavity, and the Darcy equation was used to describe the flow in porous medium. Applying the formula for the pressure field near a single spherical cavity, they developed an analytical formula for permeability of a vuggy porous medium.

Recently, Arbogast et al. [3,7,8] modeled the vuggy porous medium on the fine scale using Stokes equations in the vugs, Darcy's law in the porous rock, and the Beavers-Joseph-Saffman boundary condition on the interface between the two regions. By using the tools from homogenization theory, they obtained a macroscopic Darcy's law governing the medium on coarse scale. In order to evaluate the effective coarse scale permeabil-

ity, a mixed finite element formulation with a single set of basis functions that applied for the entire Darcy-Stokes system on fine scale has been developed.

Another similar upscaling approach was recently presented by Popov et al. [9–11]. The Stokes-Brinkman equations, rather than the Darcy-Stokes equations, were used on the fine scale to compute upscaled effective permeability of fractured karst carbonate reservoirs based on homogenization theory. The Stokes-Brinkman equations can be reduced to either the Stokes or the Darcy equations by appropriate choice of parameters and avoid the explicit formulation of the boundary conditions at the fluid/porous interfaces. In their study, the fractures were treated as free-flow regions as same as vugs. This approach provided an accurate model. But it was not practical due to a large number of grids required because of two different length scales (matrix/vug size and fracture thickness).

Above discussion shows that the main difficulty of numerical upscaling calculation of equivalent permeability for fractured vuggy porous medium exists in the first step, i.e., how to model the fluid flow in fractured vuggy porous media efficiently. The objectives of this study are (1) to propose a new conceptual model to model the fluid flow in fractured vuggy porous media efficiently on fine scale; (2) to develop a theoretical upscaling method to estimate the equivalent permeability of fractured vuggy porous medium from the fine scale to the coarse scale.

Towards these goals, we firstly consider the fractured vuggy rock as a composite porous medium, consisting of fractures system, matrix system, and vugs system. The flow in matrix and fractures systems follows Darcy law, and the vugs system is considered as free-flow region in which Stokes equations are considered. With these assumptions, in Section 2 we derive a new conceptual model namely discrete fracture-vug network (DFVN) model and its mathematical formulation, which is an extension of classic discrete fracture model of fractured porous media. In Section 3.1, via a two-scale homogenization limit as period tends to zero, we obtain an equivalent macroscopic Darcy's law governing the medium on coarse scale. A mixed finite element numerical formulation for homogenization equations is developed in Section 3.2. Finally, the equivalent permeability of some fractured vuggy porous media with typical rock fabrics has been analyzed in Section 4. At the end, the applicability and validity of the method for these more general fractured vuggy systems are assessed through a simple test of the coarse-scale model.

## 2 Discrete fracture-vug network model on fine scale

As observed in carbonate formation, three porosity types (matrix, fractures, and vugs) are typically presented in naturally fractured vuggy porous media. These fractures and vugs distribute irregularly and vary in size, from microscopic to macroscopic. Several continuum conceptual models are proposed to study the flow behavior through such media in [12–14]. In the DFVN conceptual model, the fractures and vugs are embedded in porous rock, and the isolated vugs are connected via discrete fracture networks

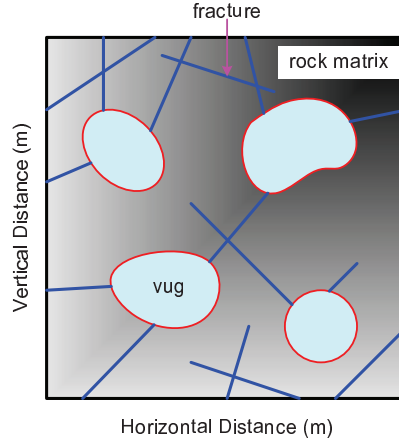


Figure 2: Conceptualization of fractured vuggy porous medium as a DFVN model, with fractures system, vugs system and porous rock matrix system.

(cf. Fig. 2). Furthermore, we conceptualize fractured vuggy porous media as composite porous materials, consisting of (1) fractures system, (2) matrix system, and (3) vugs system. The flow in matrix and fractures follows Darcy law, and the vugs are free-flow region. In this paper, we consider the fluid flow is isothermal, single phase, and incompressible with constant fluid viscosity, and all rock properties, e.g. permeability and initial porosity, are constant.

## 2.1 Free-flow region

Considering the creeping flow of an incompressible Newtonian fluid in the vugs, the Stokes equation, used to describe the free-flow, has the form

$$\nabla \cdot \mathbf{u} = 0, \quad (2.1)$$

$$-\mu \nabla^2 \mathbf{u} + \nabla p_s = \rho \mathbf{f}, \quad (2.2)$$

where  $\mathbf{u}$  is fluid velocity (m/s),  $\nabla$  is gradient operator,  $\mu$  is fluid viscosity (Pa·s),  $p_s$  is pressure in free-flow region (Pa),  $\rho$  is density ( $\text{kg}/\text{m}^3$ ),  $\mathbf{f}$  is body force per unit mass ( $\text{m}/\text{s}^2$ ). The first expression is the mass continuity equations, and the second is the balance of momentum. Also, recall the incompressible Newtonian fluid stress tensor which is given by the formula

$$\boldsymbol{\sigma} = -p_s \mathbf{I} + 2\mu \mathbf{S}(\mathbf{u}), \quad (2.3)$$

where  $\mathbf{I}$  is unit tensor, and  $\mathbf{S}(\mathbf{u})$  is strain rate

$$\mathbf{S}(\mathbf{u}) = \frac{1}{2} (\nabla \mathbf{u} + \mathbf{u} \nabla). \quad (2.4)$$

The boundary conditions for Eqs. (2.1) and (2.2) can be classified into two types: Dirichlet (velocity) and Neumann (traction) conditions [15–17] as follows

$$\mathbf{u} = \mathbf{u}_D, \quad \text{on } \Gamma_D, \quad (2.5)$$

$$\mathbf{n} \cdot \boldsymbol{\sigma} = \mathbf{t}_N, \quad \text{on } \Gamma_N, \quad (2.6)$$

where  $\mathbf{u}_D$  is the specific velocity on Dirichlet boundary  $\Gamma_D$ ,  $\mathbf{n}$  is the outward unit normal vector of boundary,  $\mathbf{t}_N$  is the specific traction. No-slip boundary conditions are specified on the impermeable wall of the open fluid domain. Traction-free boundary conditions are imposed on the outlet surface. The conditions at the interface between the free-flow region and porous medium need to be handled carefully; details of such interfacial conditions will be presented in Section 2.3.

## 2.2 Porous flow region

For the matrix system, which is a typical porous flow region, one has the classical Darcy law, along with conservation of mass

$$\nabla \cdot \mathbf{v} = 0, \quad (2.7)$$

$$\mu(\mathbf{K})^{-1} \mathbf{v} + \nabla p_d = \rho \mathbf{f}, \quad (2.8)$$

where  $\mathbf{v}$  is Darcy velocity i.e. the volume average velocity (m/s),  $\mathbf{K}$  is the permeability tensor ( $\text{m}^2$ ), and  $p_d$  is the pore average pressure (Pa).

In the former study [9–11], the fractures were explicitly treated as free-flow regions as same as vugs. This approach provided an accurate model, but it was not practical due to a large number of grids required because of two different length scales (matrix/vugs' size and fractures' aperture). In fact, the fluid flow model in the fracture could be simplified to a parallel plate laminar flow model with non-slip boundary condition. And then it could be described as the form of Darcy formula with the equivalent flow rate i.e. cubic law [18]. So the fractures system could be considered as porous flow region like rock matrix; and the Eqs. (2.7) and (2.8) could be written separately for the porous matrix and the fractures.

Based on this equivalent concept, all variables remain constant in the lateral direction (along aperture); and the fluid flow along aperture direction is neglected. So the fractures are geometrically simplified by using ( $d-1$ )-dimensional entities in a  $d$ -dimensional domain. In other words, in 2D space, the fractures are represented by the linear entities, which are 1D (cf. Fig. 3) [19–21]. To examine this idea, we consider a portion of a porous medium that includes one fracture (cf. Fig. 3). The whole porous flow region is represented by  $\Omega_d$ , which includes the porous rock matrix  $\Omega_m$  and the macro fractures  $\Omega_f$ . Let CEQ represent the flow control equations Eqs. (2.7) and (2.8). According to Fig. 3, the integral form of these equations for the original model (single-porosity model) can be written as

$$\int_{\Omega_d} \text{CEQ} \, d\Omega = \int_{\Omega_m} \text{CEQ} \, d\Omega_m + \int_{\Omega_f} \text{CEQ} \, d\bar{\Omega}_f. \quad (2.9)$$

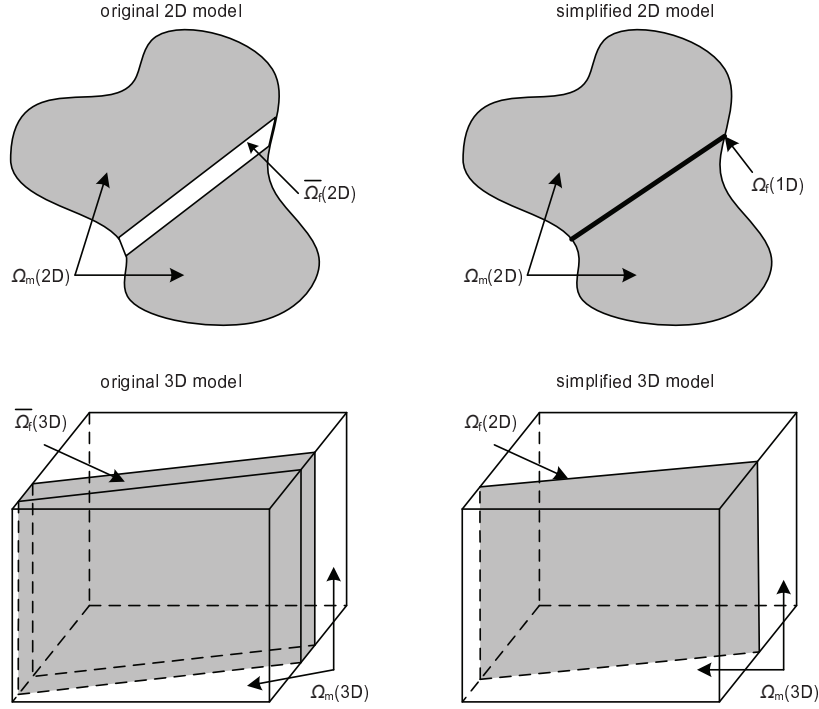


Figure 3: Schematic representation of discrete fracture approximation.

The same integral form for the discrete fracture model is written as

$$\int_{\Omega_d} CEQ \, d\Omega = \int_{\Omega_m} CEQ \, d\Omega_m + e \times \int_{\Omega_f} CEQ \, d\Omega_f, \tag{2.10}$$

where  $e$  is the fracture aperture (or thickness).

This simplification removes the length-scale contrast caused by the explicit representation of the fracture aperture as in Popov’s study. As a result, computational efficiency is improved considerably. The boundary conditions for equations Eq. (2.7) and Eq. (2.8) can also be classified into two types: Dirichlet (pressure) and Neumann (fluid flux) conditions, expressed as

$$p_d = p_D, \quad \text{on } \Gamma_D, \tag{2.11}$$

$$\mathbf{n} \cdot \frac{\mathbf{K}}{\mu} (\nabla p_d - \rho \mathbf{f}) = q_N, \quad \text{on } \Gamma_N, \tag{2.12}$$

where  $p_d$  is the specific pressure on Dirichlet boundary  $\Gamma_D$ ,  $q_N$  is a specific value or expression of the inward Darcy flux (m/s) on Neumann boundary  $\Gamma_N$ .

### 2.3 Interfacial boundary conditions

The problem then remains in defining relevant boundary conditions at the interface between the two regions. It is clear that the mass and momentum must be balanced across the interface between the free flow region and porous medium. Continuity of normal stress tensor and normal velocity (i.e. mass conservation) are robust and generally accepted boundary conditions expressed as

$$\mathbf{u} \cdot \mathbf{n} = \mathbf{v} \cdot \mathbf{n}, \quad \text{on } \Sigma, \quad (2.13)$$

$$\mathbf{n} \cdot (-\boldsymbol{\sigma} \cdot \mathbf{n}) = \mathbf{n} \cdot (p_d \mathbf{I} \cdot \mathbf{n}), \quad \text{on } \Sigma. \quad (2.14)$$

Then, the natural choices regarding the tangential velocity component would be either that it vanishes on low permeable porous wall or that it is continuous for large permeability. However, both turn out to be inaccurate, as shown for instance by the experiments of Beavers et al. [22,23]. They proposed a discontinuity condition in the interfacial tangential velocity, which is proportional to the shear rate of the free fluid, i.e.,

$$u_s - v_d = \frac{\sqrt{K}}{\alpha} \frac{\partial u_s}{\partial y}, \quad \text{on } \Sigma, \quad (2.15)$$

where  $y$  is the direction perpendicular to the interface,  $u_s$  is the Stokes velocity calculated in free-flow region,  $v_d$  is Darcy velocity calculated in porous medium and  $K$  is the permeability. The dimensionless slip coefficient  $\alpha$  characterizes the structure of the permeable material near its interface with the free flow region. Saffman [24] justified this law theoretically, and showed that the term involving  $v_d$  could be dropped. Jones [25] reinterpreted this law so that it applied to curved boundaries and non-tangential flows by formulating the boundary condition in terms of the tangential component of the fluid stress tensor as follows

$$\mathbf{u} \cdot \boldsymbol{\tau} = \frac{\sqrt{\boldsymbol{\tau} \cdot \mathbf{K} \cdot \boldsymbol{\tau}}}{\mu \alpha} (-\boldsymbol{\sigma} \cdot \mathbf{n}) \cdot \boldsymbol{\tau}, \quad \text{on } \Sigma, \quad (2.16)$$

where  $\boldsymbol{\tau}$  is the unit tangential vector of boundary. For Newtonian fluid, the interfacial boundary conditions Eq. (2.14) and Eq. (2.16) can be simplified to

$$2\mu \mathbf{n} \cdot \mathbf{S}(\mathbf{u}) \cdot \mathbf{n} = p_s - p_d, \quad \text{on } \Sigma, \quad (2.17)$$

$$\mathbf{u} \cdot \boldsymbol{\tau} = -2 \frac{\sqrt{\boldsymbol{\tau} \cdot \mathbf{K} \cdot \boldsymbol{\tau}}}{\alpha} \mathbf{n} \cdot \mathbf{S}(\mathbf{u}) \cdot \boldsymbol{\tau}, \quad \text{on } \Sigma. \quad (2.18)$$

Here the expression (2.17), namely so-called Beavers-Joseph-Saffman (BJS) condition, is supported by other independent work [26–28]. And the suggested values range of  $\alpha$  is between 0.01 and 4.

### 3 Upscaling and numerical implementation

#### 3.1 Upscaling based on homogenization

In this section, we consider the upscaling of the DFVN model from the fine scale to the coarse scale based on homogenization theory. The main idea of homogenization theory is to replace a real heterogeneous structure with effective or equivalent properties which has the same average macroscopic behavior [29]. The short summary presented next is based on two-scale asymptotic expansion (cf., e.g., [30–33]).

For ease of presentation we assume that the overall domain  $\Omega$  is Lipschitz and bounded in  $\mathbb{R}^2$ . And the geometric domain  $\Omega$  is periodic of period  $\varepsilon Y$ , where  $Y$  is a base cell for the periodic tiling of unit volume  $|Y|$ . Let  $\Omega_s^\varepsilon$  be the free-flow region,  $\Omega_d^\varepsilon$  the porous flow region and  $\Sigma^\varepsilon$  the interface between two. Let  $\mathbf{n}_s$  be the outer unit normal vector to  $\Sigma^\varepsilon$ , and  $\boldsymbol{\tau}_s$  be a unit tangent to  $\Sigma^\varepsilon$ . The DFVN model on fine scale satisfies the following set of equations.

##### Free-flow region (Stokes equation)

$$-\mu\varepsilon^2\nabla^2\mathbf{u}^\varepsilon + \nabla p_s^\varepsilon = \rho\mathbf{f}, \quad \text{in } \Omega_s^\varepsilon, \quad (3.1)$$

$$\nabla \cdot \mathbf{u}^\varepsilon = 0, \quad \text{in } \Omega_s^\varepsilon. \quad (3.2)$$

##### Porous flow region (Darcy equation)

$$\mu\mathbf{K}^{-1}\mathbf{v}^\varepsilon + \nabla p_d^\varepsilon = \rho\mathbf{f}, \quad \text{in } \Omega_d^\varepsilon, \quad (3.3)$$

$$\nabla \cdot \mathbf{v}^\varepsilon = 0, \quad \text{in } \Omega_d^\varepsilon. \quad (3.4)$$

##### Interfacial boundary conditions

$$\mathbf{u}^\varepsilon \cdot \mathbf{n}_s = \mathbf{v}^\varepsilon \cdot \mathbf{n}_s, \quad \text{on } \Sigma^\varepsilon, \quad (3.5)$$

$$2\mu\varepsilon^2\mathbf{n}_s \cdot \mathbf{S}(\mathbf{u}^\varepsilon) \cdot \mathbf{n}_s = p_s^\varepsilon - p_d^\varepsilon, \quad \text{on } \Sigma^\varepsilon, \quad (3.6)$$

$$\mathbf{u}^\varepsilon \cdot \boldsymbol{\tau}_s = -2\frac{\varepsilon\sqrt{\boldsymbol{\tau}_s \cdot \mathbf{K} \cdot \boldsymbol{\tau}_s}}{\alpha}\mathbf{n}_s \cdot \mathbf{S}(\mathbf{u}^\varepsilon) \cdot \boldsymbol{\tau}_s, \quad \text{on } \Sigma^\varepsilon. \quad (3.7)$$

##### Outer boundary conditions

$$\mathbf{u}^\varepsilon = 0, \quad \text{on } \partial\Omega \cap \partial\Omega_s^\varepsilon, \quad (3.8)$$

$$\mathbf{v}^\varepsilon \cdot \mathbf{n} = 0, \quad \text{on } \partial\Omega \cap \partial\Omega_d^\varepsilon. \quad (3.9)$$

The homogenization problem is to determine the behavior of the system as  $\varepsilon \rightarrow 0$ . In order to ensure the existence of limitation of pressure and velocity as  $\varepsilon \rightarrow 0$ , in the equations we have scaled both the viscosity  $\mu$  and the permeability tensor  $\mathbf{K}$  by  $\varepsilon^2$  [3, 30]. And the permeability of porous medium is also required to multiply a similar scaling factor. These considerations then are imposed to the interfacial boundary conditions Eqs. (3.6)

and (3.7). We assume that there is a Representative Element of Volume (REV) which features both porous and fluid domains. As ansatz, a formal asymptotic expansion of the type

$$\mathbf{u}^\varepsilon(\mathbf{x}) = \sum_{i=0}^{\infty} \varepsilon^i \mathbf{u}_i(\mathbf{x}, \mathbf{y}) = \mathbf{u}_0(\mathbf{x}, \mathbf{y}) + \varepsilon^1 \mathbf{u}_1(\mathbf{x}, \mathbf{y}) + \varepsilon^2 \mathbf{u}_2(\mathbf{x}, \mathbf{y}) + \dots, \quad (3.10)$$

$$\mathbf{v}^\varepsilon(\mathbf{x}) = \sum_{i=0}^{\infty} \varepsilon^i \mathbf{v}_i(\mathbf{x}, \mathbf{y}) = \mathbf{v}_0(\mathbf{x}, \mathbf{y}) + \varepsilon^1 \mathbf{v}_1(\mathbf{x}, \mathbf{y}) + \varepsilon^2 \mathbf{v}_2(\mathbf{x}, \mathbf{y}) + \dots, \quad (3.11)$$

$$p_s^\varepsilon(\mathbf{x}) = \sum_{i=0}^{\infty} \varepsilon^i p_s^i(\mathbf{x}, \mathbf{y}) = p_s^0(\mathbf{x}, \mathbf{y}) + \varepsilon^1 p_s^1(\mathbf{x}, \mathbf{y}) + \varepsilon^2 p_s^2(\mathbf{x}, \mathbf{y}) + \dots, \quad (3.12)$$

$$p_d^\varepsilon(\mathbf{x}) = \sum_{i=0}^{\infty} \varepsilon^i p_d^i(\mathbf{x}, \mathbf{y}) = p_d^0(\mathbf{x}, \mathbf{y}) + \varepsilon^1 p_d^1(\mathbf{x}, \mathbf{y}) + \varepsilon^2 p_d^2(\mathbf{x}, \mathbf{y}) + \dots \quad (3.13)$$

is substituted in Eqs. (3.1)-(3.9). Firstly one obtains that the first term in the pressure expansions does not depend on the fine-scale variable  $\mathbf{y}$ , that is

$$p^0(\mathbf{x}) = p_s^0(\mathbf{x}) = p_d^0(\mathbf{x}), \quad \text{on } \Omega. \quad (3.14)$$

Next, one obtains a set of cell problems that are used to compute the equivalent (or upscaled) permeability of the REV. Let  $d$  be the dimension (2 or 3) and  $\mathbf{e}_j$  be a unit vector in the  $j$ -th direction. And then the  $d$  cell problems can be obtained, i.e.

$$-\nabla_{\mathbf{y}}^2 \mathbf{w}_s^j + \nabla_{\mathbf{y}} \pi_s^j = \mathbf{e}_j, \quad \text{in } \mathbf{Y}_s, \quad (3.15)$$

$$\nabla_{\mathbf{y}} \cdot \mathbf{w}_s^j = 0, \quad \text{in } \mathbf{Y}_s, \quad (3.16)$$

$$\mathbf{K}^{-1} \mathbf{w}_d^j + \nabla_{\mathbf{y}} \pi_d^j = \mathbf{e}_j, \quad \text{in } \mathbf{Y}_d, \quad (3.17)$$

$$\nabla_{\mathbf{y}} \cdot \mathbf{w}_d^j = 0, \quad \text{in } \mathbf{Y}_d, \quad (3.18)$$

$$\mathbf{w}_s^j \cdot \mathbf{n}_s = \mathbf{w}_d^j \cdot \mathbf{n}_s, \quad \text{on } \Sigma, \quad (3.19)$$

$$2\mathbf{n}_s \cdot \mathbf{S}(\mathbf{w}_s^j) \cdot \mathbf{n}_s = \pi_s^j - \pi_d^j, \quad \text{on } \Sigma, \quad (3.20)$$

$$\mathbf{w}_s^j \cdot \boldsymbol{\tau}_s = -2 \frac{\sqrt{\boldsymbol{\tau}_s \cdot \mathbf{K} \cdot \boldsymbol{\tau}_s}}{\alpha} \mathbf{n}_s \cdot \mathbf{S}(\mathbf{w}_s^j) \cdot \boldsymbol{\tau}_s, \quad \text{on } \Sigma, \quad (3.21)$$

where  $\mathbf{w}_l^j$  and  $\pi_l^j$  ( $l = s, d$ ) are the  $\mathbf{Y}$ -periodic vector fields. The macroscopic equivalent permeability  $\boldsymbol{\kappa}$  is then computed by averaging the fine-scale velocities

$$\boldsymbol{\kappa} = \frac{1}{|\mathbf{Y}|} \left( \int_{\mathbf{Y}_s} \mathbf{w}_s^j \, d\mathbf{y} + \int_{\mathbf{Y}_d} \mathbf{w}_d^j \, d\mathbf{y} \right), \quad (3.22)$$

and its components are given as

$$\kappa_{ij} = \frac{1}{|\mathbf{Y}|} \left( \int_{\mathbf{Y}_s} (\mathbf{w}_s^j)_i \, d\mathbf{y} + \int_{\mathbf{Y}_d} (\mathbf{w}_d^j)_i \, d\mathbf{y} \right),$$

where

$$\int_{Y_d} (w_d^j)_i d\mathbf{y} = \int_{Y_m} (w_m^j)_i d\mathbf{y} + e \times \int_{Y_f} (w_f^j)_i d\mathbf{y}, \quad m=\text{matrix}, f=\text{fracture}.$$

The macroscopic equivalent flux is given by the Darcy's law on coarse scale as  $\varepsilon \rightarrow 0$

$$\mu(\kappa)^{-1} \bar{\mathbf{u}} + \nabla p^0 = \rho \mathbf{f} \quad (3.23)$$

and subject to conservation of mass

$$\nabla \cdot \bar{\mathbf{u}} = 0. \quad (3.24)$$

Note that  $w^j, j=1, \dots, d$  ( $d=2$  or  $3$ ) in Eqs. (3.15)-(3.18) are the fine-scale velocities in the base cell, that is  $Y$ , and are subject to unit forcing in the respective direction. Since  $\mathbf{e}_j$  can also be transferred to the pressure term, as follows

$$\nabla_y (\pi_l^j - y_j) = \nabla_y \pi_l^j - \mathbf{e}_j. \quad (3.25)$$

One can consider the velocity  $w^j$  as the results over a unit pressure drop in the  $j$ -th coordinate in base cell along with periodic boundary conditions. Above procedure is very similar to the one employed for upscaling the Stokes-Darcy equations in a vuggy porous media. The reader is thus referred to [3, 11] for technical details.

### 3.2 Numerical implementation

There exist a number of studies which aim at developing efficient methods for Darcy-Stokes problem and Darcy-Brinkman problem [7, 8, 34–37]. In this paper, we use a mixed finite element method in the porous flow and free-flow domains and special transition elements near the interface to allow for tangential discontinuities. A multigrid method has been designed to solve the resulting saddle point linear system. For more details on these types of numerical scheme, the reader is referred to [7, 8].

The treatment with fractures is the key point in DFVN model. Let's recall the Fig. 2, the DFVN model could be decomposed into two parts (the free-flow region and the porous flow region). In our study, the porous flow region is described as a discrete fracture model, in which the fluid flow in fractures is demonstrated as a narrow high-permeable  $(d-1)$ -dimensional region based on equivalent concept (cf. Section 2.2). First the geometry is discretized using triangular elements for the matrix and line elements for the fractures in 2D problem (cf. Fig. 4). In the numerical implementation proceeding for porous flow region, the superposition principle has been used to couple the rock matrix and fractures (for details, cf. Fig. 5).

## 4 Examples and discussion

In this section, we consider the solution of the homogenized cell problem (3.15)-(3.21), and in particular the equivalent permeability that results from the formula (3.22). At

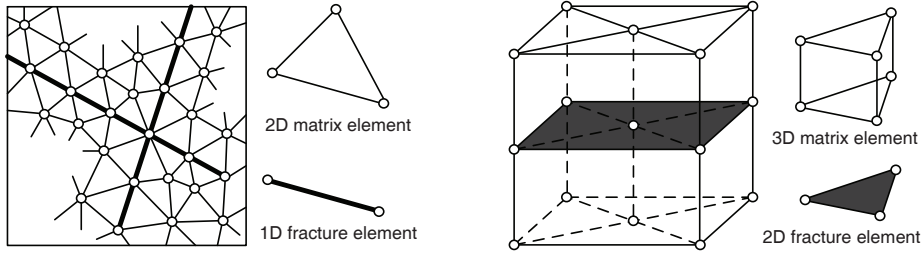


Figure 4: Schematic of matrix and fracture elements.

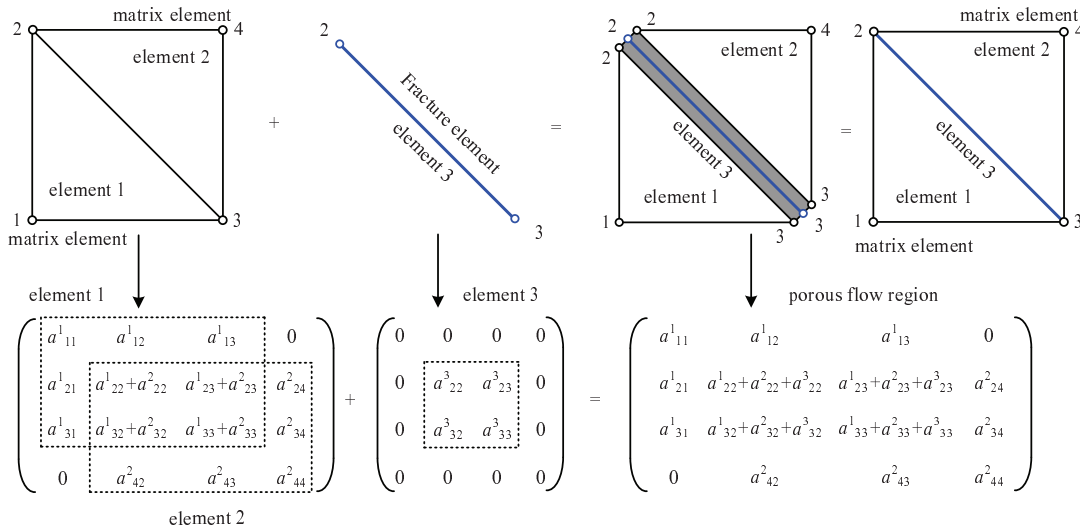


Figure 5: Schematic of FEM implementation for matrix and fracture elements.

first, a simple layered medium was conducted in Section 4.1. Analytical solutions based on the BJS interfacial conditions are derived, which are used to estimate the accuracy of our numerical calculation. Next the equivalent permeability for a porous medium with a single vug has been discussed. In Section 4.2, the impacts of the vug size, shape, and location on the equivalent permeability also have been investigated. In Section 4.3, we calculated the equivalent permeability for the porous medium with different fracture-vug networks. At last the applicability of the method to the scale up of more general system was assessed.

### 4.1 A layered porous medium

We begin with a study of a layered medium, which has a square base cell  $Y = (-L/2, L/2) \times (-L/2, L/2)$  with  $Y_s = (-L/2, L/2) \times (-b/2, b/2)$  and  $Y_d = Y - Y_s$ , as illustrated in Fig. 6. The base case of our studies in this part is an 8 cm  $\times$  8 cm ( $L = 8$  cm) sample with slip

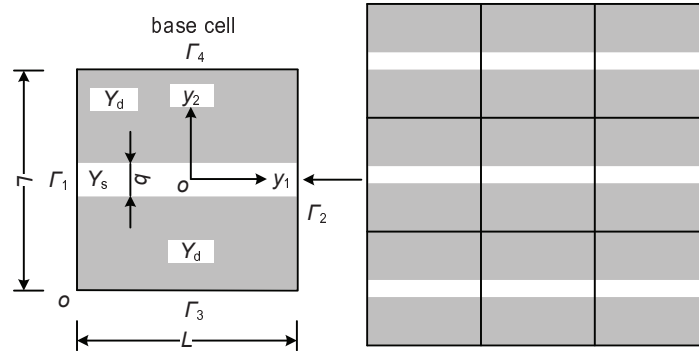


Figure 6: A layered porous medium.

coefficient  $\alpha = 1.0$ , homogeneous isotropic rock matrix's permeability  $K_m = 10$  mD, and vugs with  $b = 1$ cm. Since this problem can be solved analytically (see Appendix), this example can be viewed more as an estimation of the accuracy of our numerical solution. The analytical equivalent permeability is expressed as

$$\kappa = \begin{bmatrix} \kappa_{11} & 0 \\ 0 & \kappa_{22} \end{bmatrix},$$

where

$$\kappa_{11} = \frac{1}{L} \left( \frac{1}{12} b^3 + \frac{\sqrt{K}}{2\alpha} b^2 + K(L-b) \right), \quad \kappa_{22} = \frac{L}{L-b} K.$$

At first, the impact of BJS slip coefficient  $\alpha$  on the equivalent permeability calculation of the layered medium is tabulated in Table 1. A good match with analytical and numerical solutions has been achieved, which verifies the accuracy of the finite element numerical scheme of this study. The results show that the  $\kappa_{22}$  permeability is not affected by the slip coefficient  $\alpha$  because the tangential flow does not exist in this direction. As discussion in Section 2.3, the dimensionless slip coefficient  $\alpha$  characterizes the structure of the permeable material near its interface with the free flow region, and must therefore be determined for each particular system in principle. However, the slip coefficient  $\alpha$  has small influence on the equivalent permeability if the matrix permeability  $K_m \leq 10^5$  mD (detailed analysis see Appendix).

Next, results of varying the rock matrix permeability  $K_m$  are given in Table 2. The results show again the excellent agreement between analytical and our numerical solutions. And then a more interesting experiment is designed to vary the vug aperture  $b$ . Results are shown in Table 3. It can be seen that permeability component  $\kappa_{11}$  is much larger than the rock permeability with the increase of vug aperture. Large aperture vugs usually result in  $\kappa_{11}$  of a million to a billion times greater than that of the rock matrix permeability. However, the influence of vug aperture on  $\kappa_{22}$  is relatively small. When the

Table 1: Impact of different Beavers-Joseph-Saffman slip coefficient  $\alpha$  on the equivalent permeability of the layered medium.

$\alpha$	$\kappa_{11}$ (mD)		$\kappa_{22}$ (mD)	
	analytical	this work	analytical	this work
0.01	1.0479167E+09	1.0479170E+09	11.4285714	11.42857
0.1	1.0422917E+09	1.0422920E+09	11.4285714	11.42857
1	1.0417292E+09	1.0417290E+09	11.4285714	11.42857
10	1.0416729E+09	1.0416730E+09	11.4285714	11.42857
100	1.0416673E+09	1.0416670E+09	11.4285714	11.42857

Table 2: Effect of varying the rock matrix permeability  $K_m$  for the layered medium.

$K_m$ (mD)	$\kappa_{11}$ (mD)		$\kappa_{22}$ (mD)	
	analytical	this work	analytical	this work
1	1.041686E+09	1.041687E+09	1.142857143	1.142857
10	1.041729E+09	1.041729E+09	11.42857143	11.42857
100	1.041864E+09	1.041865E+09	114.2857143	114.2857
1000	1.042293E+09	1.042293E+09	1142.857143	1142.857

Table 3: Effect of varying the vug aperture  $b$  for the layered medium.

$b/L$	$\kappa_{11}$ (mD)		$\kappa_{22}$ (mD)	
	analytical	numerical	analytical	numerical
0.001	547.32333	547.31990	10.01001	10.01001
0.01	5.3374323E+05	5.3374320E+05	10.10101	10.10101
0.05	6.6676676E+07	6.6676680E+07	10.52632	10.52632
0.125	1.0417292E+09	1.0417290E+09	11.42857	11.42857
0.5	6.6667667E+10	6.6667900E+10	20.00000	19.99999
0.9	3.8880324E+11	3.8880810E+11	100.0000	99.99986
1	5.3333333E+11	5.3334570E+11	5.333333E+11	5.333457E+11

aperture of vug tends to zero, namely the vug disappears,  $\kappa_{11}$  and  $\kappa_{22}$  achieve the minimum that are equal to rock permeability  $K_m$ . As the ratio  $b/L$  approaches 1, i.e., the vug is full of the overall base cell, then  $\kappa_{11}$  and  $\kappa_{22}$  achieve the maximum with  $5.3334 \times 10^{11}$  mD.

## 4.2 Porous medium with a single vug

### 4.2.1 Medium with a circular vug

Fig. 7 depicts a homogeneous and isotropic porous medium with a circular vug. The dimensions of base cell is  $Y = (-L/2, L/2) \times (-L/2, L/2)$ , where  $Y_s$  represents vug,  $Y_d$  represents porous medium.  $L$  is the length of base cell;  $r$  is the radius of circular vug. The matrix permeability  $K_m = 10$  mD, and  $L = 1$  m. In this case, the equivalent permeability is diagonal due to the symmetric structure, with  $\kappa_{11} = \kappa_{22}$ . Results of different vug radius

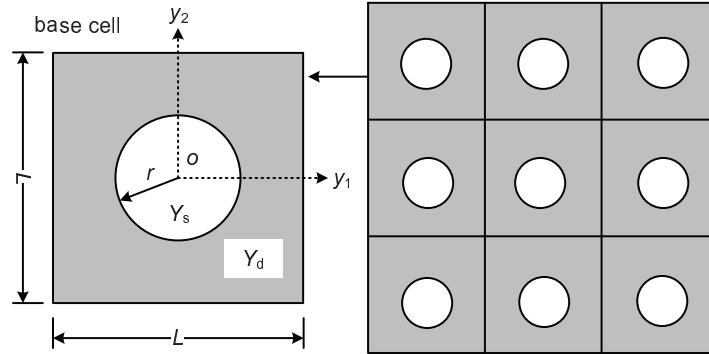


Figure 7: Porous medium with a circular vug.

Table 4: The equivalent permeability of base cell with different vug radius.

$2r/L$	$\kappa_{11} = \kappa_{22}$ (mD)		
	$\alpha = 0.1$	$\alpha = 1.0$	$\alpha = 10.0$
0.02	1.000628E+01	1.000627E+01	1.000627E+01
0.1	1.015803E+01	1.015807E+01	1.015803E+01
0.2	1.064756E+01	1.064751E+01	1.064774E+01
0.4	1.287336E+01	1.287336E+01	1.287336E+01
0.6	1.790391E+01	1.790382E+01	1.790388E+01
0.8	3.104431E+01	3.104436E+01	3.104398E+01
0.98	1.374829E+02	1.374829E+02	1.374823E+02
1	7.024635E+07	7.018975E+07	7.018408E+07

and slip coefficients are shown in Table 4. It is clear that, with the increase of vug radius, the equivalent permeability increases, but has the same order of magnitude of matrix permeability. When the vug diameter  $2r$  approaches to the length of base cell  $L$ , the equivalent permeability increases rapidly and improves 6 orders of magnitude of  $K_m$ . It again shows that the calculation is not affected by the slip coefficient  $\alpha$ .

The two cases above show that the permeability is strongly influenced by the size of vug. Both two examples indicate that, when the vugs are connected with each other through base cells, the equivalent permeability would increase several orders of magnitude of  $K_m$ . However this is not expected when the vugs do not form channels. Such medium with disconnected vugs, i.e., a free-flow region completely surrounded by rock matrix, have the similar orders of magnitude of rock matrix permeability. So the vug connectivity is the most critical variable in predicting equivalent permeability.

#### 4.2.2 Effect of vug shape and location

At first, an evaluation of the geometric dependence of the homogenized permeability tensor is demonstrated with four basic shapes: square, disk, hexagon, and cross-shape,

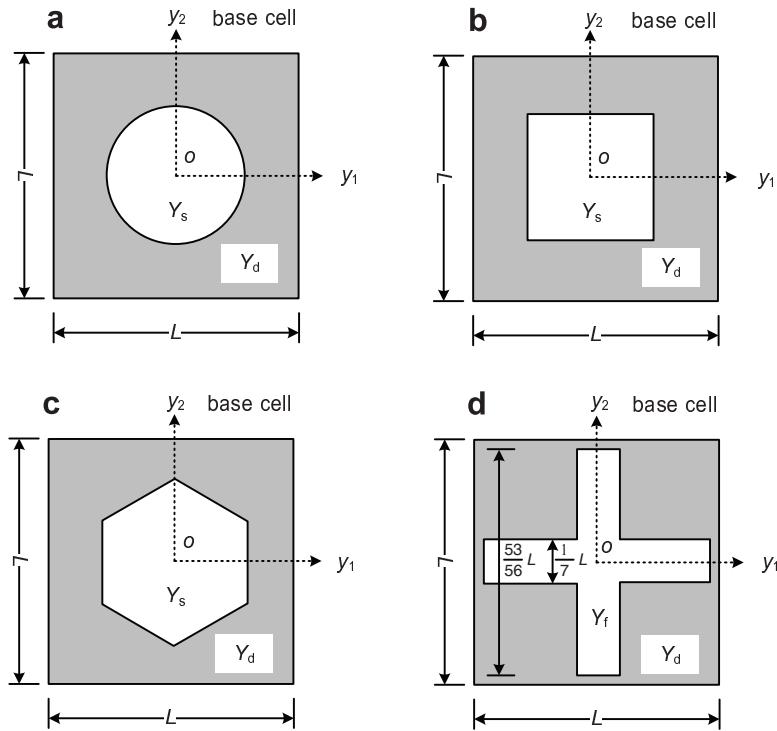


Figure 8: Four base cells with different shape vug: (a) disk, (b) square, (c) hexagon, (d) cross-shape.

which are shown in Figs. 8(a)-(d). The length of base cell  $L = 1$  m, and in all cases the area of  $Y_s$  is  $1/4$ . Furthermore, the geometric symmetry of square and disk ensures that the equivalent permeability tensor will be a scalar multiple of the identity.

The computed equivalent permeabilities with different shape vug and rock matrix permeability are displayed in Table 5 (in all cases, the slip coefficient  $\alpha = 1.0$ ). In order to study the effect of different shapes for the base cell, the percentage differences relative to the square cell are calculated: (1) disk cell approximates  $-3.01\%$ ; (2) hexagon cell approximates  $-2.10\%$ , (3) cross-shape cell approximates  $187.7\%$ . It suggests that the effective permeability with a concave vug is quite different to that of convex vug. The shape of vug has important impacts on the effective permeability. The results in Table 6 suggest that it is independent on the location of vug (in this Table the matrix permeability  $K_m = 100$  mD).

In Fig. 9, the solutions of Darcy-Stokes equations for cell problems (3.15)-(3.21) with different shape vug are displayed. The velocity  $w^j$  is plotted in Figs. 9(a)-(d). And the pressure profiles of  $\pi^j$  are shown in Figs. 9(e)-(h). The numerical results indicate that the velocity and pressure distribution throughout the base cell should be symmetric or antisymmetric, and the physical quantities take equal values on the opposite sides of the base cell due to the periodic boundary conditions.

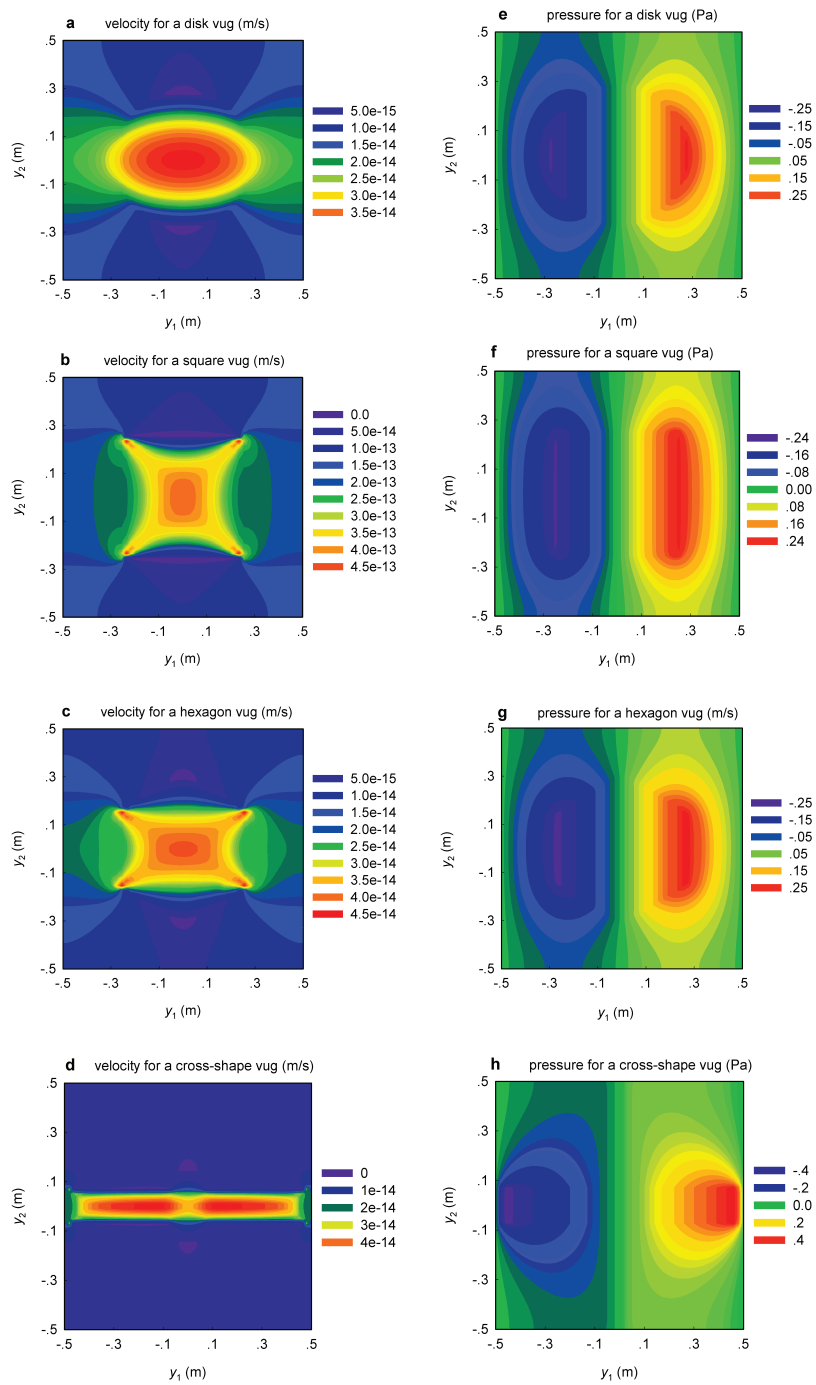


Figure 9: Variations in the velocity  $w^j$  (along  $y_1$ -direction) and the pressure  $\pi^j$  of base cell with different shape vug based on periodic boundary conditions: (a)-(d) velocity profiles; (e)-(h) pressure profiles. Properties:  $K_m=10$  mD,  $\mu=1$  Pa·s, slip coefficient  $\alpha=1.0$ .

Table 5: Homogenized permeability tensors obtained with different matrix permeability for the three representative cells shown in Fig. 8.

$K_m$ (mD)	$\kappa_{11}$ (mD)			
	disk	square	hexagon	cross-shape
0.1	1.6676E-01	1.7195E-01	1.6832E-01	4.9469E-01
1	1.6676E+00	1.7195E+00	1.6832E+00	4.9469E+00
10	1.6676E+01	1.7195E+01	1.6832E+01	4.9469E+01
100	1.6676E+02	1.7195E+02	1.6832E+02	4.9469E+02

Table 6:  $\kappa_{11}$  of three representative cells with different vug location, shown in Fig. 8.

location of vug center (m)	$\kappa_{11}$ (mD)		
	disk	square	hexagon
(0.0, 0.0)	1.66757E+02	1.71948E+02	1.68322E+02
(0.1, 0.0)	1.66757E+02	1.71957E+02	1.68327E+02
(0.0, 0.1)	1.66757E+02	1.71969E+02	1.68324E+02
(0.1, 0.1)	1.66757E+02	1.72174E+02	1.68323E+02

### 4.3 Porous medium with fracture-vug network

In this section, the equivalent permeability of a base cell is computed for four different types of fracture-vug networks. A base cell with three large elliptical vugs imbedded inside the rock matrix is considered. A fracture network connecting to the vugs is established. Four cases are illustrated in Fig. 10. And the bold black lines represent fractures;  $L = 1$  m; the homogeneous and isotropic permeability  $K_m$  of rock matrix region  $Y_d$  is 10 mD; all fractures' aperture  $a = 2$  mm; radius of circular vug  $r = 0.1$  m, semi-major axis of elliptical vug  $r_1 = 0.25$  m, semi-minor axis of elliptical vug  $r_2 = 0.1$  m.

Table 7 shows the equivalent permeability tensor of four typical base cells. As expected, case (a) is similar to the previous sections. The equivalent permeability increased by 25%-45% computed to the rock matrix permeability. Since vugs are connected via fractures in case (b), its equivalent permeability tensor improves 200%-300% to the rock matrix permeability. However, the order of magnitude of equivalent permeability is the same as that of surrounding porous rock. When the fluid flows through the two typical base cells above, the fluid can not enter the vugs and fractures directly but needs to pass through the rock matrix, thus the matrix determines the order of magnitude of the overall matrix permeability.

The calculation of case (c) shows that the equivalent permeability is about six orders of magnitude more than the matrix permeability in the horizontal direction (i.e.  $y_1$ -direction). The vertical (i.e.  $y_2$ -direction) permeability is same as that of case (b). The large increase in horizontal direction is due to the fact that most of the fluids flow runs directly through the fractures and the rock matrix contributes very little to the overall flow rate. This is again verified by the case (d), in which both the horizontal and vertical permeabilities improve six orders of magnitude of the matrix permeability. Note that

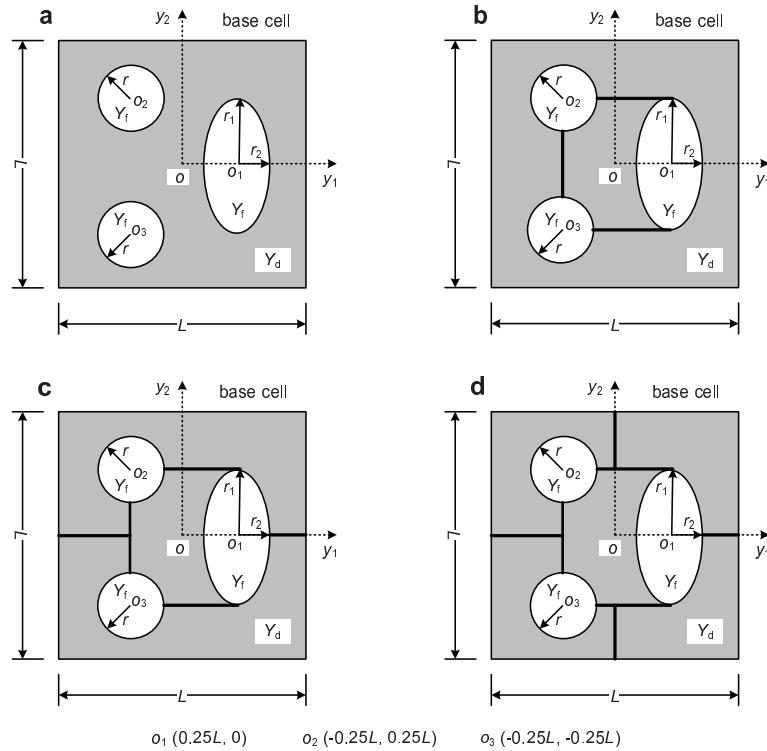


Figure 10: Base cells with different fracture-vug networks: (a) isolate vugs i.e. ignoring all the fractures, (b) fractures connecting to vugs but not to the boundary of base cell, (c) fractures connecting to vugs and to the boundary of base cell only in  $y_1$ -direction, (d) fractures connecting to vugs and to the boundary of base cell both in  $y_1$ -direction and  $y_2$ -direction.

Table 7: The equivalent permeability tensor of four typical base cells in Fig. 10.

base cell types	equivalent permeability tensor $\kappa$ (mD)
Case (a)	$\begin{pmatrix} 12.7307 & 0 \\ 0 & 14.6830 \end{pmatrix}$
Case (b)	$\begin{pmatrix} 36.4326 & 0 \\ 0 & 29.8007 \end{pmatrix}$
Case (c)	$\begin{pmatrix} 19.8282 \times 10^5 & 0 \\ 0 & 29.8057 \end{pmatrix}$
Case (d)	$\begin{pmatrix} 19.8282 \times 10^5 & 42.1934 \\ 42.1934 & 8.6050 \times 10^5 \end{pmatrix}$

the offdiagonal components of case (d) are non-zero due to the incompletely symmetric base cell. The above results show that the connectivity of the fracture-vug network has an important influence on the equivalent permeability, especially for those discrete fracture-vug networks connecting to each other in overall domain.

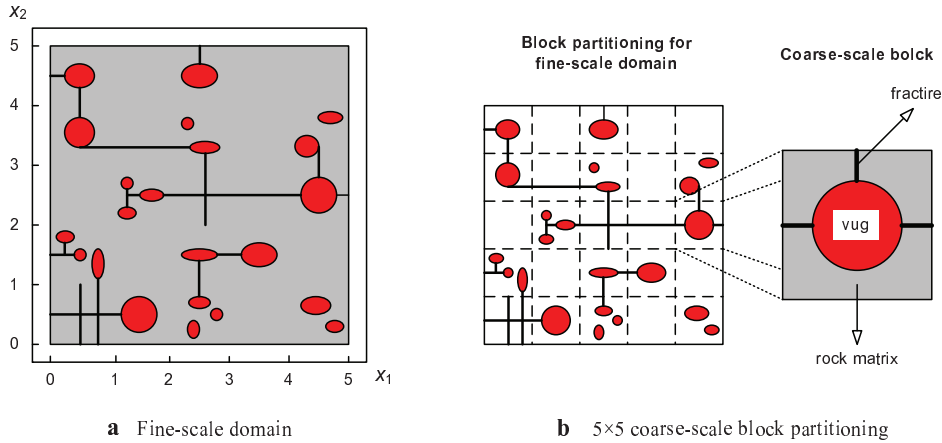


Figure 11: Fine-scale domain (a) consisting of rock matrix and discrete fracture-vug networks. The coarse-scale block partitioning (b) used for numerical calculations of equivalent permeability.

#### 4.4 A simple computation test of the coarse-scale model

In practice, for full field-scale problems, we need to solve the Darcy macro-model (3.23)-(3.24) on a coarse grid, using equivalent permeability (3.22) upscaling from the fine scale Darcy-Stokes cell problem (3.15)-(3.21). The objective of this section is to illustrate this procedure. Then we compare a fine-scale reference solution of Eqs. (3.15)-(3.21) with the coarse-scale model (3.23)-(3.24) to verify the validity of the proposed upscaling method and the accuracy of the calculation for equivalent permeability. We consider a fine-scale domain populated with some discrete fracture-vug networks, illustrated in Fig. 11. The sample is 5 m by 5 m square, and we divide it into a coarse scale grid of  $5 \times 5$  blocks (so the grid blocks are 1 m by 1 m square). The background permeability of rock matrix is homogeneous and isotropic with  $K_m = 10$  mD, the fluid viscosity  $\mu = 1$  Pa·s, and the BJS slip coefficient  $\alpha = 1.0$ . We consider no flow at top and bottom sides of the domain (Fig. 11(a)). The flow is driven by a unit pressure drop in the horizontal ( $x_1$ ) direction. This is achieved by imposing a 5 Pa pressure at the left side and zero at the right side of the domain. The fine scale solution is displayed in Fig. 12(a).

We next solve the reference cell problem (3.15)-(3.21) for the equivalent permeability (3.22). For each coarse scale grid block, the upscaled permeability is computed using periodic boundary conditions. In Fig. 12(b), we plot the corresponding coarse scale pressure. We have compared this coarse scale pressure with the averaged coarse scale pressure obtained from the fine scale solution. The relative  $L_2$  error was found to be less than 10%. The comparisons of pressure profiles at various  $y$  or  $x$  locations are plotted in Fig. 13. The coarse scale results are about conformable to the fine scale results with the relative  $L_2$  errors (1) 7.081% at  $x = 0.5$ , (2) 10.786% at  $y = 3.5$ , (3) 4.966% at  $y = 1.0$ . These results indicate that the proposed method to calculate the equivalent permeability for fractured vuggy porous medium is valid and applicable.

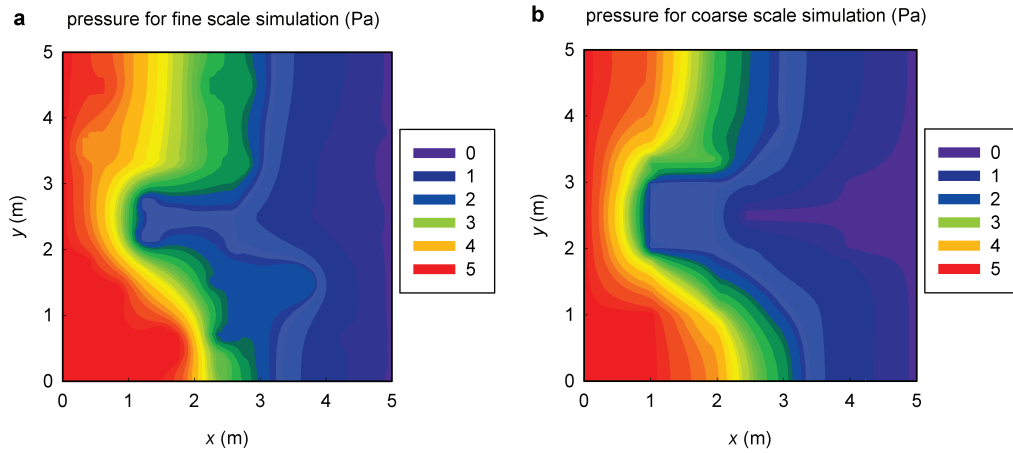


Figure 12: Comparison of the fine scale (a) and coarse scale (b) pressure solutions.

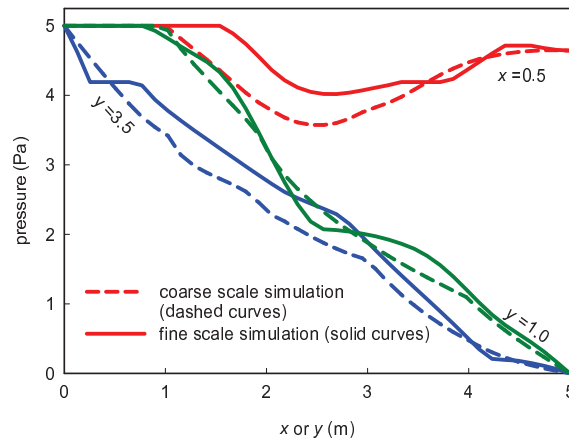


Figure 13: Comparison of the fine scale (solid curves) and coarse scale (dashed curves) pressure profiles at various values of  $y$  and  $x$ .

## 5 Conclusions

Equivalent permeability provides a valid prescription of large scale flow through fractured vuggy porous medium. In this paper, a new conceptual model, i.e., discrete fracture-vug network model has been proposed. And we have developed a general numerical method to accurately compute this equivalent permeability tensor based on this new model and homogenization theory. Our brief study allows us to make several important conclusions about modeling fluid flow in fractured vuggy media.

First, the calculation results show that the presence of fractures and vugs can increase the overall permeability. The equivalent permeability, as computed from (3.22) and cell

problem (3.15)-(3.21), is mildly sensitive to the location of the vug, but is very sensitive to the size and shape of vugs, and extremely sensitive to the connectivity of fractures and vugs. When the fluids flow in a fractured vuggy porous medium in which the vugs and fractures are not well connected, the equivalent permeability remains the same order of magnitude of matrix permeability. However, a connected fracture-vug systems could increase the equivalent permeability by many orders of magnitude. Thus the connectivity of the discrete fracture-vug network is the dominant consideration in understanding the flow in fractured vuggy porous media.

Second, the simple computation test case of Section 4.4 supports the overall validity of the coarse scale model of (3.23)-(3.24). Usually natural fractured vuggy porous media are not periodic, thus the periodic boundary condition is problematic in that periodic repetitions of base cell may artificially destroyed the connectivity of the fracture-vug network. Thus, when upscaling fractured vuggy porous media, in order to improve the accuracy of calculation, the coarse scale grid should maintain the topology of the fracture-vug network (cf. Fig. 11(b)).

Third, the discrete fracture-vug network model provides a natural way of modeling fluids flow through fractured vuggy porous media. Due to the simplification of fractures, the computation efficiency of this model improves greatly. The use of finite element technique for the calculation of equivalent permeability allows for the accurate modeling of complex discrete fracture-vug network models. The dimensionless slip coefficient has small influence on the equivalent permeability when the matrix permeability  $K_m \leq 10^5$  mD. Thus  $\alpha = 1.0$  in this paper is reasonable.

## Acknowledgments

This work was supported by National Basic Research Program of China (973 Program), "Study the Fundamentals of the Carbonate Karst Reservoir Development 2006CB202404" and Important National Science and Technology Project of China (2008ZX05014-005-003 HZ). We are also grateful for the fruitful discussions with Dr. Zisheng Wang and Prof. Hengmu Shu during the course of this work.

## Appendix

Consider Darcy-Stokes system that consists of a channel of width  $b$  limited above and below by a homogeneous isotropic porous medium (see Fig. 6). The flow in the channel satisfies the Stokes equation, and the flow in the porous medium obeys Darcy' law.

Firstly, we assume that a uniform pressure gradient  $-\delta p/L$  is maintained in the longitudinal direction  $y_1$  in both the channel  $Y_s$  and the permeable materials  $Y_d$ . So if we ignore all the body forces, the velocity field does not depend on the  $y_1$ -coordinate. Let  $u(y_2)$  denote the velocity of the fluid along the  $y_1$ -coordinate. The Stokes equation for the velocity field in the channel and the corresponding Beavers-Joseph-Saffman conditions

are written as

$$-\mu u''(y_2) - \frac{\delta p}{L} = 0, \tag{A.1}$$

$$u\left(-\frac{b}{2}\right) = \frac{\sqrt{K}}{\alpha} u'\left(-\frac{b}{2}\right), \tag{A.2}$$

$$u\left(\frac{b}{2}\right) = -\frac{\sqrt{K}}{\alpha} u'\left(\frac{b}{2}\right), \tag{A.3}$$

and the solution is

$$u(y_2) = \left(-\frac{y_2^2}{2} + \frac{\sqrt{K}}{2\alpha}b + \frac{b^2}{8}\right) \frac{\delta p}{\mu L}. \tag{A.4}$$

The average velocity in the channel along  $y_2$ -coordinate is

$$\bar{u} = \frac{1}{b} \int_{-b/2}^{b/2} u(y_2) dy = \left(\frac{\sqrt{K}}{2\alpha}b + \frac{b^2}{12}\right) \frac{\delta p}{\mu L}. \tag{A.5}$$

On the other hand, Darcy's law implies that

$$v = \frac{K}{\mu} \frac{\delta p}{\mu L}. \tag{A.6}$$

For the base cell problem, both the pressure gradient along  $y_1$ -direction and viscosity are unit amount. And then through calculating the total average velocity of Stokes and Darcy flow throughout the base cell, the equivalent permeability components related to  $y_1$ -direction can be obtained

$$\kappa_{11} = \frac{1}{L} \left(\frac{1}{12}b^3 + \frac{\sqrt{K}}{2\alpha}b^2 + K(L-b)\right), \quad \kappa_{12} = 0. \tag{A.7}$$

The similar analytical process is conducted to calculate the equivalent permeability components related to  $y_2$ -direction. We also assume that a same pressure drop  $-\delta p$  is exerted along  $y_2$ -direction, and that the flow is stationary. In the porous materials, a uniform fluid flow along  $y_2$ -direction is expected. On the other hand, because the fluid velocity out from porous medium into vug is uniform, the viscous force does not exist. Thus the velocity and pressure is constant in vug because the fluid meets no resistance in the vug. So the velocity in the overall base cell is uniform and equals the Darcy velocity of porous medium, expressed as follows

$$u = \frac{LK}{L-b} \frac{\delta p}{\mu L}. \tag{A.8}$$

And then the equivalent permeability components related to  $y_2$ -direction can be obtained

$$\kappa_{22} = \frac{L}{L-b} K, \quad \kappa_{21} = 0. \tag{A.9}$$

From the above discussion, we can find that the slip coefficient  $\alpha$  only affects the fluid flow in vug or free-flow region. So we can analyze the following ratio

$$\lambda = \frac{\frac{\sqrt{K}b^2}{2\alpha}}{\frac{1}{12}b^3} = \frac{6\sqrt{K}}{\alpha b}. \quad (\text{A.10})$$

Here we let

$$\lambda \leq 0.05 \Rightarrow K \leq \left(\frac{5\alpha b}{6}\right)^2 \times 10^{-4}. \quad (\text{A.11})$$

As discussed in Section 1, the vugs usually are macroscopic and their diameters are greater than or equal to 0.01 m, here we specify the width of vug  $b = 0.01$  m and  $\alpha = 1.0$ . Then we can obtain

$$K \leq 6.944 \times 10^{-9} \text{ m}^2 (6.944 \times 10^6 \text{ mD}). \quad (\text{A.12})$$

Therefore, if the permeability is less than  $(6.944 \times 10^6 \text{ mD})$  which is the common case in oil-field, the slip coefficient  $\alpha$  has little impact on the calculation of permeability and  $\alpha = 1.0$  in this study is reasonable.

## References

- [1] F. J. Lucia, Carbonate Reservoir Characterization, Springer-Verlag Berlin Heidelberg, 2007.
- [2] S. Eezybek and S. Akin, Pore network modeling of multiphase flow in fissured and vuggy carbonates, SPE paper 113384, presented at the 2008 SPE/DOE Improved Oil Recovery Symposium, Tulsa, Oklahoma, USA, 19-23 April, 2008.
- [3] T. Arbogast and L. H. Lehr, Homogenization of a Darcy-Stokes system modeling vuggy porous media, Comput. Geosci., 10(3) (2006), 291-302.
- [4] A. F. Gulbransen, V. L. Hauge, and K. A. Lie, A multiscale mixed finite-element method for vuggy and naturally-fractured reservoirs, SPE paper 119104, presented at the 2009 SPE Reservoir Simulation Symposium, Woodlands, Texas, USA, 2-4 February, 2009.
- [5] T. Arbogast, D. S. Brunson, S. L. Bryant et al., A preliminary computational investigation of a macro-model for vuggy porous media, In Computational Methods in Water Resources XV, New York, Elsevier, 2004.
- [6] G. H. Neale and W. K. Nader, The permeability of a uniformly vuggy porous medium, SPE J., 13(2) (1973), 69-74.
- [7] T. Arbogast and D. S. Brunson, A computational method for approximating a Darcy-Stokes system governing a vuggy porous medium, Comput. Geosci., 11 (2007), 207-218.
- [8] T. Arbogast and M. S. M. Gomez, A discretization and multigrid solver for a Darcy-Stokes system of three dimensional vuggy porous media, Comput. Geosci., 13 (2009), 331-348.
- [9] P. Popov, G. Qin, L. Bi, et al., Multiscale methods for modeling fluid flow through naturally fractured carbonate karst reservoirs, SPE paper 110778, presented at the 2007 SPE Annual Technical Conference and Exhibition, Anaheim, California, USA, 11-14 November, 2007.
- [10] P. Popov, L. F. Bi, Y. Efendiev, et al., Multiphysics and multiscale methods for modeling fluid flow through naturally fractured carbonate reservoirs, SPE paper 105378, presented at the 15th SPE Middle East Oil & Gas Show and Conference, Bahrain, 11-14 March, 2007.
- [11] P. Popov, Y. Efendiev, and G. Qin, Multiscale Modeling and Simulations of Flows in Naturally Fractured Karst Reservoirs, Commun. Comput. Phys., 6(1) (2009), 162-184.

- [12] Z. J. Kang, Y. S. Wu, J. L. et al., Modeling multiphase flow in naturally fractured vuggy petroleum reservoirs, SPE paper 102356, presented at the 2006 SPE Annual Technical Conference and Exhibition, San Antonio, Texas, USA, 24-27 September, 2006.
- [13] Y. S. Wu, G. Qin, R. E. Ewing, et al., A multiple-continuum approach for modeling multiphase flow in naturally fractured vuggy petroleum reservoirs, SPE paper 104173, presented at the 2006 SPE International oil & Gas Conference and Exhibition, Beijing, China, 5-7 December, 2006.
- [14] Y. S. Wu, G. Qin, Z. J. Kang, et al., A triple-continuum pressure-transient model for a naturally fractured vuggy reservoir. SPE paper 110044, presented at the 2007 SPE Annual Technical Conference and Exhibition, Anaheim, California, USA, 11-14 November, 2007.
- [15] O. C. Zienkiewicz and R. L. Taylor, *The Finite Element Method Volume 3: Fluid Dynamics*, New York, McGraw-Hill, 2000.
- [16] J. N. Reddy and D. K. Gartling, *The Finite Element Method in Heat transfer and Fluid dynamics*, New York, CRC, 2000.
- [17] J. Donea and A. Huerta, *Finite Element Methods for Flow Problems*, England, John Wiley & Sons Ltd, 2003.
- [18] P. A. Witherspoon, J. S. Y. Wang, K. Iwai, and J. E. Gale, Validity of Cubic Law for Fluid Flow in a Deformable Rock Fracture, *Water Resour. Res.*, 16(6) (1980), 1016-1024.
- [19] J. Kim and M. Deo, Finite element discrete fracture model for multiphase flow in porous media, *AIChE J.*, 46(6) (2000), 1120-1130.
- [20] M. Karimi-Fard and A. Firoozabadi, Numerical simulation of water injection in 2D fractured media using discrete-fracture model, *SPE J.*, 4 (2003), 117-126.
- [21] H. Hoteita and A. Firoozabadi, An efficient numerical model for incompressible two-phase flow in fractured media, *Adv. in Water Resour.*, 31 (2008), 891-905.
- [22] G. S. Beavers and D. D. Joseph, Boundary condition at a naturally permeable wall, *J. Fluid Mech.*, 30 (1967), 197-207.
- [23] G. S. Beavers, E. M. Sparrow, and R. A. Magnuson, Experiments on coupled parallel flows in a channel and a bounding porous medium, *J. Basic Eng.*, 92D (1970), 843-848.
- [24] P. G. Saffman, On the boundary condition at the surface of a porous medium, *Stud. Appl. Math.*, 1 (1971), 93-101.
- [25] I. P. Jones, Low Reynolds number flow past a porous spherical shell, *Cambridge Philosophical Society, Proceedings*, 73 (1973), 231-238.
- [26] G. I. Taylor, A model for the boundary conditions of a porous material, Part 1. *J. Fluid Mech.*, 49 (1971), 319-326.
- [27] G. Dagan, Generalization of Darcy law for nonuniform flows, *Water Resour. Res.*, 15 (1979), 1-7.
- [28] M. Sahraoui and M. Kaviani, Slip and no-slip velocity boundary conditions at interface of porous, plain media, *Int. J. Heat and Mass Transfer*, 35 (1992), 927-944.
- [29] A. Benssousan, J. L. Lions, and G. Papanicoulau, *Asymptotic Analysis for Periodic Structures*, Amsterdam, North Holland, 1978.
- [30] E. Sanchez-Palencia, *Non-Homogeneous Media and Vibration Theory*, volume 127 of *Lecture Notes in Physics*, Springer-Verlag Berlin, 1980.
- [31] O. A. Oleinik, *On homogenization problems*, *Trends and Applications of Pure Mathematics to Mechanics*, Springer Berlin, 1984.
- [32] V. V. Zhikov, S. M. Kozlov, and O. A. Oleinik, *Homogenization of Differential Operators and Integral Functionals*, Springer-Verlag Berlin, 1994.
- [33] U. Hornung, *Homogenization and Porous Media*, Springer New York, 1997.

- [34] A. Salinger, R. Aris and J. Derby, Finite element formulations for large-scale, coupled flows in adjacent porous and open fluid domains, *Int. J. Numer. Meth. Fluids*, 18(12) (1994), 1185-1209.
- [35] D. K. Gartling, C. E. Hickox, and R. C. Givler, Simulation of coupled viscous and porous flow problems, *Comput. Fluid Dyn.*, 7(1) (1996), 23-48.
- [36] W. J. Layton, F. Schieweck, and I. Yotov, Coupling fluid flow with porous media flow, *SIAM. J. Numer. Anal.*, 40 (2003), 2195-2218.
- [37] H. Tan and K. M. Pillai, Finite element implementation of stress-jump and stress-continuity conditions at porous-medium, clear-fluid interface, *Computers and Fluids*, 38 (2009), 1118-1131.